Plasmon-Mediated Energy Transfer between Two Systems out of Equilibrium

Camilo R Pérez de la Vega, Elise Bailly, Kévin Chevrier, Benjamin Vest, Jean-Paul Hugonin, Antoine Bard, Alban Gassenq, Clémentine Symonds, Jean-Michel Benoit, Joel Bellessa, et al.

Plasmon mediated energy transfer between two systems out of equilibrium

Camilo R. Pérez de la Vega[#,†] Elise Bailly[#,‡] Kévin Chevrier[#,†] Benjamin Vest,[‡] Jean-Paul Hugonin,[‡] Antoine Bard,[¶] Alban Gassenq,[¶] Clémentine Symonds,[¶] Jean-Michel Benoit,[¶] Joel Bellessa,[¶] Jean-Jacques Greffet,[*,‡] Yannick De Wilde,[*,†] and Valentina Krachmalnicoff[*,†]

†*Institut Langevin, ESPCI Paris, Université PSL, CNRS, 75005 Paris, France*

‡*Université Paris-Saclay, Institut d'Optique Graduate School, CNRS, Laboratoire Charles Fabry, 91127, Palaiseau, France*

¶*Institut Lumière Matière, Université Lyon 1, Villeurbanne 69100, France*

E-mail: jean-jacques.greffet@institutoptique.fr; yannick.dewilde@espci.fr; valentina.krachmalnicoff@espci.fr

Abstract

The fabrication of nanostructured samples assembling organic, inorganic emitters and plasmons has been widely explored in the last decades in the context of energy harvesting applications or for the design of optoelectronic devices. However, understanding the interaction between each component in such a complex scenario is a challenge. Here we report on the energy transfer between ensembles of inorganic quantum dots and organic J-aggregates mediated by surface plasmon polaritons. The two emitters' species

[#] These authors contributed equally to this work.

are spatially separated on the surface of a continuous silver film in an optically structured sample in order to measure the impact of their relative separation on the energy transfer. We introduce a theoretical model of the photoluminescence of the system to quantify the energy transfer between the two species through the chemical potential of photons.

Keywords

Surface plasmons - energy transfer - strong coupling - Local Kirchhoff's law - organic-inorganic emitters - photoluminescence - Brendel Borman model

Introduction

Coupling organic and inorganic materials has brought a lot of attention in the last decades for various purposes such as energy harvesting in solar cells,[1] hot electron transfer,[2] photocatalysis[3] and optoelectronic devices.[4] Hybrid devices of these materials are appealing to overcome their limitations when used separately.[5] On one hand, organic materials, such as J-aggregated molecules, show a large absorption cross section, high oscillator strength and thus strong light-matter interaction. On the other hand, inorganic materials, such as quantum dots (QDs), are photostable, have enhanced optical non-linearity and high electrical conductivity. In the case of quantum dots, the emission spectrum is rather narrow band and the maximum emission wavelength is directly related to the QDs' diameter, which makes them very versatile fluorescent nano-objects. Enabling energy transfer between organic and inorganic materials merges together the best of both worlds, as it has been shown in the recent literature.[6] One approach to increase the efficiency as well as the range of the energy transfer is to shape a favouring electromagnetic environment of the materials e.g. embedding the materials in a microcavity,[7–10] creating electromagnetic hotspots with metallic nanoparticles[11,12] or surface plasmon polaritons.[13,14] However, understanding the role played by the

different components is a hard task, due to the formation of hybrid modes, and to the spatial and spectral overlap between emitters' ensembles and plasmonic modes. Note also that ensembles of emitters cannot be considered as a mere superposition of independent single emitters, and an appropriate theoretical model has to be used.[15]

In this paper, we explore a multilayer system in which organic (J-aggregated TDBC) and inorganic (QDs) ensembles of fluorescent emitters interact with a surface plasmon polariton (SPP) propagating over a distance of a few microns. The interaction of SPPs' confined field and large oscillator strength of organic molecules results in the formation of hybrid extended modes and the observation of light-matter strong coupling.[16,17] We take advantage of the micrometric propagation length of the SPP to spatially separate regions in which the inorganic material interacts with the SPP to regions in which it interacts with strongly coupled hybrid modes. This modulates the energy transfer between the inorganic material and the organic material via surface polaritons modes. Numerical simulations based on the local Kirchhoff's law to model light emission by an ensemble of thermalized emitters[18] enable to quantify the energy transfer between the two ensembles of fluorescent emitters through SPP coupling. More precisely, we introduce a chemical potential to characterize quantitatively the energy transfer to the molecules. Simulations are in very good agreement with the experiments.

Description of the sample and the experimental method

The sample under study is sketched in Fig.1a and its fabrication is detailed in the Methods section. It consists of a $t_{\mathrm{Jagg}} = 17$ nm thick layer of J-aggregated TDBC deposited on top of a $t_{\mathrm{Ag}} = 50$ nm thick silver film laying on a glass coverslip. Then, we deposited on top a $t_{\mathrm{QD}} = 15$ nm thick layer of QDs embedded in a polymer matrix of PMMA. The thicknesses above are measured with an Atomic Force Microscope (AFM). We measure the photoluminescence (PL) of the system in the reciprocal space to visualize the available

electromagnetic modes through their dispersion relation.

The spectral properties of each ensemble of emitters on glass are presented in Fig.1b. The absorption and PL spectra of the J-aggregates are narrow and their maxima are centered at 585 nm and 595 nm respectively. The QDs absorption spectrum is characterized by a large band increasing towards short wavelengths and an exciton resonance at 526 nm while the QDs PL spectrum has a maximum at $\lambda_{\mathrm{QDs}} = 576\,\mathrm{nm}$ and partially overlaps the absorption spectrum of the J-aggregates making our system suitable for observing energy transfer effects. The presence of the silver layer modifies the spectra with respect to the spectra obtained on glass. The experimental reflectance of the complete sample, which is reported in Fig. 1c, shows the presence of the so-called lower polariton (LP) and upper polariton (UP) branches that anticross indicating a strongly coupled system.[19] The anticrossing occurs at the resonance between the J-aggregates exciton (at 2.1 eV) and the SPPs propagating at the interface between the silver and the two dielectric layers, with a corresponding Rabi splitting of 153 meV.

In such a multilayer sample, energy transfer between the different layers influences the optical properties of the entire system. Understanding the role played by each layer in the definition of the optical properties and in the energy transfer is a complex task. To disentangle the contribution of the different components, we study a sample where the J-aggregated TDBC is prepared in a non-absorbing state. By comparing the optical properties obtained when the excitation laser illuminates a region in which J-aggregates are photobleached with the optical properties obtained in a region in which they are not, energy transfer can be studied. Moreover, we study samples shown in Fig. 2a. consisting in a disk with photobleached TDBC molecules surrounded by the system with non photobleached molecules. We excite the QDs at the center of the disk so that the energy transfer between the QDs and the TDBC molecules can be studied as a function of the radius of the disk. This study can assess the possibility of surface plasmon mediated energy transfer.

Locally photobleached J-aggregates areas are obtained by shining a high intensity UV

irradiation laser writer ($\lambda = 365\,\mathrm{nm}$)[20] on the J-aggregated TDBC layer before the deposition of the QDs. Photobleached J-aggregates have been shown to have the same refractive index as the active dye film, except in the spectral region around 2.1 eV where the absorption peak is removed.[17] An optical microscopy image of the sample after irradiation is shown in Fig. 2a. The circular photobleached areas (CPAs) have a diameter ranging from 1 to 10 μm by steps of 1 μm and two larger diameters of 20 and 40 μm. As 40 μm is significantly larger than the SPP propagation length (set to 2.21 µm at 570 nm, defined as 1/(2k"), see Methods), the central area of the later sample can be taken as a reference medium whose properties are not influenced by the J-aggregated TDBC.

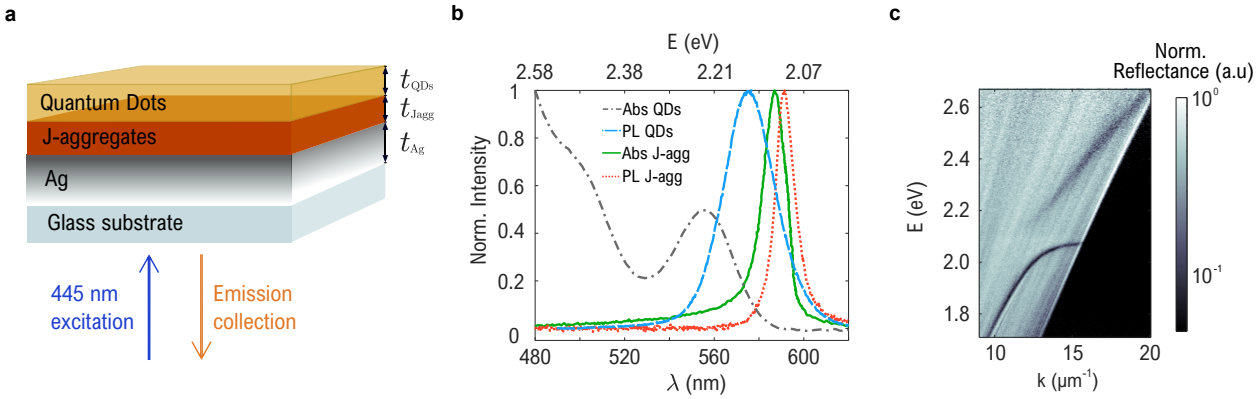

Figure 1: a) Sketch of the multilayered sample consisting of a silver film of $t_{\mathrm{Ag}} = 50\,\mathrm{nm}$, a J-aggregates layer of $t_{\mathrm{Jagg}} = 17\,\mathrm{nm}$, and a QDs/PMMA layer of $t_{\mathrm{QDs}} = 15\,\mathrm{nm}$. Such values are measured with an Atomic Force Microscope (AFM) on the sample. We excite the sample with a 445 nm laser excitation through the silver film and we collect the resulting fluorescence from the same side. The excitation wavelength is chosen in a spectral region in which the absorption cross-section of the QDs is high while the one of the J-aggregated TDBC is low. b) Absorption and PL spectra of thin films of QDs and J-aggregated TDBC deposited on glass. c) Reflectometry measurement (in logarithmic scale) of the sample showing the strongly coupled polaritons with a Rabi splitting of 153 meV.

We investigate the system through the measurements of PL spectra resolved in the sample in-plane wavevector k. For this purpose, the sample sits on an inverted microscope and the patterned multilayer is excited by a pulsed laser beam ($\lambda = 445\,\mathrm{nm}$) focused on it through the glass coverslip. The laser is focused on a diffraction limited spot through a high numerical aperture oil immersion objective (NA=1.5) and the radiation leaking from

the excited propagating modes is collected through the same objective. The excitation wavelength is chosen in a spectral region in which the absorption cross-section of the QDs is high while the one of the J-aggregated TDBC is low. We collect the TM-polarized emission over a field of view of $\sim 20\,\mu$m, and image the back focal plane of the microscope objective onto the slit of a spectrometer coupled to an EMCCD. This image is dispersed by the spectrometer's diffraction grating to get the spectrum as a function of the wave-vector. The diffraction limited laser spot enables to locally excite the center of each CPA and to study the modification of the energy transfer between the QDs and the J-aggregated TDBC when the CPA radius increases. Figure 2b shows the situation when the center of a CPA is excited. In the limiting cases with $\Phi_{\mathrm{CPA}} = 40\ \mu$m and $\Phi_{\mathrm{CPA}} = 0\ \mu$m, the electromagnetic modes are either SPPs or strongly coupled polaritons respectively.

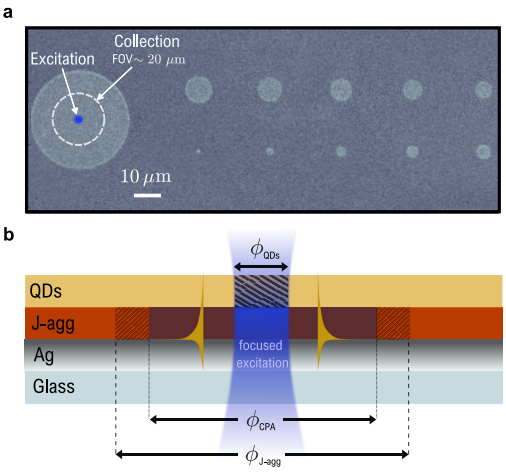

Figure 2: a) Dark-field microscopy image of a lithographed zone of the J-aggregates film deposited on silver. The design of the pattern contains circular photobleached areas (CPAs) with diameters ranging from 1 to $40\,\mu$m. The smallest separation distance between adjacent bleached regions is $20\,\mu$m to isolate them from each other. The pattern was repeated tens of times within the sample to test the repeatability of the experimental results. In the $40\,\mu$m CPA, we represented the laser excitation and the detection field of view. b) Sketch of a CPA being illuminated at its center by the focused laser excitation. Following laser excitation, QDs decay by exciting modes propagating in the sample plane. The hatched areas correspond to the volume of excited emitters in which we set a non-zero chemical potential for simulations.

Results and Discussion

Experimental results are reported on Fig. 3a-f. Let us first consider the case in which we excite an unbleached homogeneous region containing active J-aggregates topped with the layer of QDs. The corresponding PL emission spectra as a function of the wavevector is shown in the $E(k)$ map of Fig. 3a. In such region, the electromagnetic environment is shaped by the strong light-matter coupling between the J-aggregates and the SPPs, with a shift to higher wavevectors due to the layer of QDs/PMMA. The anticrossing between the LP and UP is clearly visible. Interestingly, light is emitted through the UP although it is not observable in PL measurements when only a J-aggregates layer is present as the active material on the top of a silver film.[19,21] In the case of the sample studied in this paper, since the QDs' energy spectrum overlaps the UP mode, QDs couple to it. The upper polariton then leaks into a photon. This emitter-photon interaction mediated by the polariton was first described by Hopfield.[22] The LP is also observed. In this case, two mechanisms are possible: direct emission by the QDs mediated by the LP or energy transfer from the QDs to the TDBC molecules which then emit through the LP. In what follows, we will introduce a theoretical model to analyse the data and identify the mechanism at play.

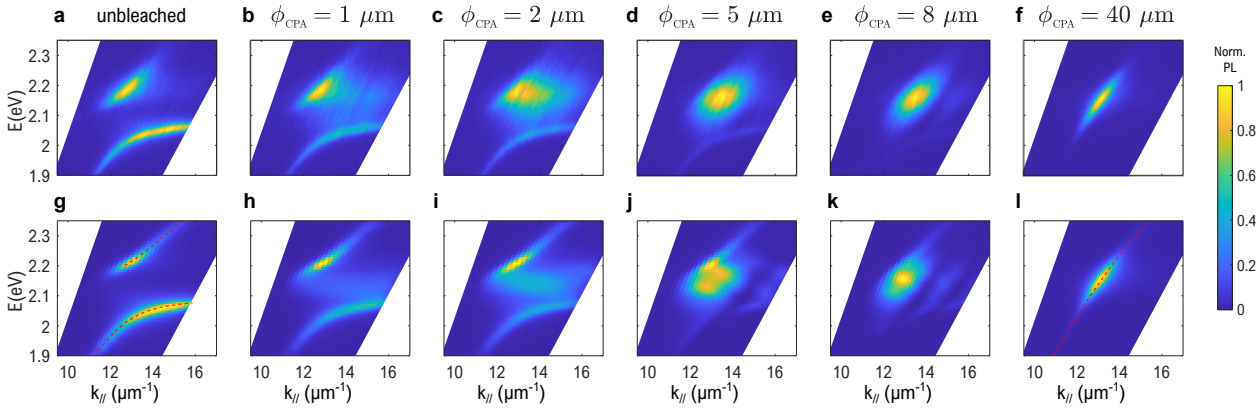

Figure 3: a)-f) Experimental and g)-l) simulated photoluminescence $E(k)$ maps for different regions in the sample. In a) and g) the laser is focused in a region where there is no lithography, i.e the J-aggregates are active. For the other subfigures, the diameter of the CPA is indicated on top of each pair of experimental and simulated results. The experiments are performed with the laser focused at the center of the CPA. The dispersion relations of the polaritons and SPPs are added in red dotted lines in g) and l) respectively.

For $\Phi_{\mathrm{CPA}} = 40$ μm, the measured PL spectrum versus k is shown in Fig. 3f. The pattern in the plane $(k_{\parallel}, E)$ indicates an emission mediated by the plasmon propagating in the system with photobleached molecules. In other words, the measurement shows no influence of the TDBC molecules indicating that there is no energy transfer between the QDs and the molecules located 20 μm apart. Given that the decay length of the SPP intensity is 2.21 μm at 570 nm, this behaviour is consistent with a QD-molecule interaction mediated by SPP.

We now turn to the intermediate cases with a CPA diameter varying between 1 and 8 μm (Fig. 3b-e). As sketched in Fig. 2b, the Gaussian laser beam excites the QDs at the center of the disk with the photobleached J-aggregates. The QDs subsequently relax through the available propagating modes. Assuming that the interaction between the QDs and TDBC molecules is mediated by surface plasmon, the distance between the excitation spot and the active J-aggregates is thus a leading feature of the system, as it rules the interaction between the QDs and the strongly coupled modes. In Figures 3b-e, light is unexpectedly detected for values of energy and k vectors at which light emission is not due to SPP, UP or LP. This is evident when comparing these data with the results obtained in the situation without CPA (Fig. 3a, f). A modification of the intensity distribution depending on Φ_{CPA} can also be noted. As the CPA radius gets larger, the J-aggregates have a smaller influence in the shape of the modes and the intensity of the LP fades.

Since the QDs emission spectrum overlaps the UP and its lower tail overlaps the LP, associating the PL at a given $E(k)$ with the emission of QDs or TDBC molecules is not straightforward. Here again, we need a theoretical model to analyse these data and identify the mechanisms responsible for the emission. We now describe the theoretical framework that enables us to analyse the data and identify the emission mechanisms. As explained in the next paragraph, a numerical simulation based on the local Kirchhoff's law enables to explain the physical processes that contribute to the detected PL.

Description of the theoretical model and comparison with the experiments

The overall PL observed in Fig. 3 a-f results from the coupling of the fluorescent emitters (both QDs and TDBC molecules) to the electromagnetic modes (SPPs, UP, LP). It also depends on the possible energy transfer between QDs and molecules. Models of light emission must account for this interplay in order to accurately predict the spectrum and directions of emission. Here, we use the local form of Kirchhoff's law which enables to model light emission by nonequilibrium systems under some conditions.[15]

Local form of Kirchhoff's law

This law states that the power $dP_{\mathrm{e}}^{(l)}(\mathbf{u},\lambda)$ emitted by an ensemble of thermalized emitters at a wavelength λ, in the solid angle $d\Omega$ around the direction given by the unit vector $\mathbf{u}$ and for a given linear polarization state l can be cast in the form:

$$dP_{\mathrm{e}}^{(l)}(\mathbf{u},\lambda) = d\lambda d\Omega \int_{\mathrm{V}} d^3\mathbf{r}' \alpha^{(l)}(-\mathbf{u},\mathbf{r}',\lambda) \frac{hc^2}{\lambda^5} \frac{1}{\exp(\frac{hc}{\lambda k_B T} - \frac{\mu(\mathbf{r}')}{k_B T}) - 1}, \tag{1}$$

where $\alpha^{(l)}(-\mathbf{u},\mathbf{r}',\lambda)\varphi_{\mathrm{inc}}\, d^3\mathbf{r}'$ is the absorption in a volume element $d^3\mathbf{r}'$ of the emitting material (QDs or TDBC molecules) illuminated by an incident plane wave coming from the reciprocal direction $-\mathbf{u}$ with a given linear polarization state l and a power flux per unit area φ_{inc}. T is the temperature and $\mu(\mathbf{r}')$ is the photon chemical potential. This quantity has been introduced in the context of semiconductor electroluminescence.[23] The photon chemical potential is then equal to the difference of the quasi Fermi levels in the valence band and the conduction band. In other words, the photon chemical potential is a characteristic of the strength of the pumping mechanism. It can be defined both for the QDs (μ_{QDs}) and for the molecules (μ_{Jagg}). It describes the number of excited emitters. It is thus a key quantity to study energy transfer between QDs and molecules. As it is shown in the Methods section, Eq. 1 can be cast in a simpler way, as a function of $\Delta\mu = \mu_{\mathrm{QDs}} - \mu_{\mathrm{Jagg}}$.

Eq. 1 shows that light emission $dP_{\mathrm{e}}^{(l)}(\mathbf{u},\lambda)$ is important when the absorptivity in the reciprocal picture $\alpha^{(l)}(-\mathbf{u},\mathbf{r}',\lambda)$ is also significant. As a consequence, some of the spectral and spatial features observed in absorption measurements can be observed in light emission measurements. In particular, the influence of a SPP or a strongly coupled mode in the emission process is accounted for by this term.

The minima of reflectivity in Fig. 1c, are a clear signature of an increased absorptivity caused by the resonant excitation of the UP and LP. It directly matches the maxima of emission in Fig. 3a. Indeed, in the reciprocal picture, the system under pumping contains molecules or quantum dots that decay by emitting light through the same surface UP and LP. Similarly, Fig. 3f shows the same emission mediated by surface plasmons. It is seen that the formula accounts for both emission mechanisms mentioned above. On one hand, an excited QD has an emission tail at low frequencies that can excite either the LP or the SPP depending on its environment. This results in a significant emission due to the leakage radiation of the surface waves which is proportional to $\exp(\frac{\mu_{\mathrm{QDs}}}{k_B T})$. On the other hand, the same QDs can transfer energy to the TDBC molecules. Then, a molecule emission proportional to $\exp(\frac{\mu_{\mathrm{Jagg}}}{k_B T})$ mediated by leakage of the LP or SPP can be observed.

The $\Delta\mu$ highlights the energy transfer between the two types of emitters

Once the values for the refractive indexes of J-aggregated TDBC, bleached J-aggregated TDBC and QDs were extracted separately from the optimization procedure described in the Methods section, we computed the photoluminescence produced by the whole system (Fig. 1a, 2a). We can then compare Fig. 3a-f to numerical simulations (Fig. 3g-l).

It was necessary to adjust $\Delta\mu$ for each CPA to fit the relative intensities between the UP and LP branches. The data of $\Delta\mu$ are presented in table 1.

Table 1: Fitted values of $\Delta\mu = \mu_{\mathrm{QDs}} - \mu_{\mathrm{Jagg}}$

	unbleached	$\Phi_{\mathrm{CPA}} = 1\mu$m	$\Phi_{\mathrm{CPA}} = 2\mu$m	$\Phi_{\mathrm{CPA}} \geq 5\mu$m
$\Delta\mu$ (meV)	270	291	295	μ_{QDs}

Since the QDs do not undergo any absorption-reemission process (See Methods section), we consider the laser spot as the only excitation source. Thus, the number of excited QDs, and hence μ_{QDs}, is the same for all CPA configurations. Consequently, a variation of $\Delta\mu$ can only be due to a variation of μ_{Jagg}, i.e. a variation of the number of excited J-aggregated molecules. The observed increase of $\Delta\mu$ when Φ_{CPA} is increased indicates a smaller number of excited TDBC molecules (i.e. a smaller μ_{Jagg}). These measurements are compatible with the picture of an energy transfer between the QDs and the J-aggregated molecules mediated by the SPPs propagating in the CPA. This process is suppressed if the SPP decay length is smaller than the CPA radius. Here, we find that for $\Phi_{\mathrm{CPA}} \geqslant 5$ μm, the energy transfer is not measured. We evaluate the SPP intensity decay length to be around 2 μm (see Methods), a value consistent with the measurements. In this latter case, only the QDs contribute to the photoluminescent emission.

Interestingly, we also observe light emitted along the dispersion relation of the UP. This is not observed without QDs, as already reported in the literature.[19] Here, the emission through the UP is due to the direct excitation of the UP electromagnetic mode by the QDs for the small values of Φ_{CPA} (see Fig. 3(a-b)). When Φ_{CPA} increases (see Fig. 3(e-f)), QDs emission is mediated by the SPP.

PL emission out of the SPP, UP and LP modes

Finally, we discuss the broad dispersion in $k_{//}$ of the emission seen in Fig. 3 b-e. It cannot be explained by invoking the sole dispersion relation of the polariton or the plasmons. The numerical simulations of Fig. 3 h-k show that the model is able to reproduce the experimental data so that this angular dependence is well captured by the sample absorptivity.

Here, we consider a particular pair $(E, k_{//})$ outside the upper polariton's dispersion relation in Fig. 4a), such as $E = 2.15$ eV and $k_{//} = 14$ $\mu\mathrm{m}^{-1}$. A physical explanation of the broad dispersion in k can be provided by analysing the effect of the presence of a CPA in real space. According to Kirchhoff's law, the emitted light is coming from regions where the

absorption proportional to $\mathrm{Im}(\epsilon)|E|^2$ is large. We thus plot the field $|\vec{E}_z|$ in the structure when illuminated by an incident plane wave from the glass side towards the sample, with this specific energy and wave vector (corresponding to an angle of 58°, and a free-space wavelength $\lambda = 576.7$ nm) in Fig. 4. We investigate the field for the two cases in which a CPA of diameter $\Phi_{CPA} = 1$ μm is present (Fig. 4b)) or absent (Fig. 4a)). We observe that when the J-aggregates are active everywhere, there is no coupling between the plane wave and any evanescent mode. In contrast, in the presence of a CPA of $\Phi_{\mathrm{CPA}} = 1$ μm the field is greatly enhanced. The CPA thus acts as an antenna, allowing to couple light in the structure for a wide range of excitation wavevectors. By reciprocity, the QDs excited in this spatial area where the field is non-zero are able to relax in the same range of wavevectors, as it is observed in the PL map of Fig. 3b. Physically these new wavewavectors originate from the diffraction of surface plasmon polaritons on the edge of the bleached TDBC area.

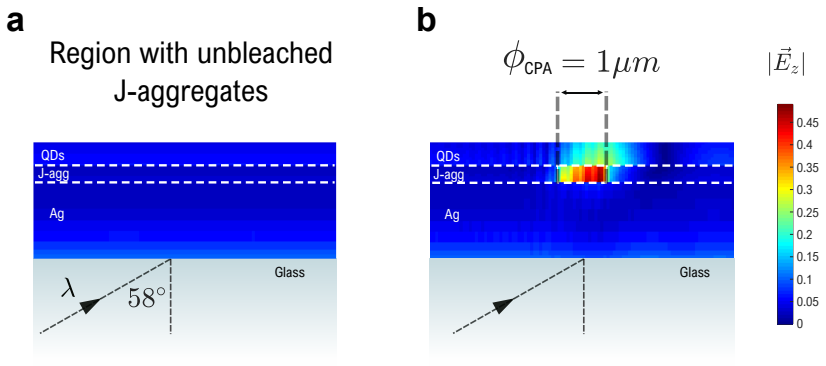

Figure 4: Maps of the field component $\vec{E}_z$ norm produced by the incidence of a TM-polarized plane wave that illuminates the sample from the glass side, with a parallel wavevector $k_{//} = 14$ $\mu\mathrm{m}^{-1}$ at 2.15 eV (i.e. at $\lambda = 576.7\,\mathrm{nm}$ and for 58°). In a), a homogeneous region (i.e far from a CPA) is illuminated and there are no excited modes which explains that the field is zero. In b), the presence of the CPA enables the coupling of the plane wave producing an intense field in its vicinity.

Conclusion

In summary, we present an approach to characterize the PL and energy transfer in systems with complex interactions between organic (J-aggregated TDBC) and inorganic (QDs)

emitters determined by light-matter coupling. By taking advantage of the microstructuration of the organic layer, the electromagnetic environment created by the hybridization of J-aggregates' emission and the SPP mode was probed with QDs as a function of the distance between emitters' ensembles. Microstructuration enables to target the QDs separately while controlling the amount of active J-aggregates in the surroundings. This results in a progressive tuning of both the shape of the propagating modes and the distribution of the intensity among them. Surprisingly, we detect light emission in the UP mode contrarily to what is normally observed in the absence of the QDs layer and also for large k-vectors for which light emission is usually forbidden. Experimental observation are thoroughly understood thanks to a theoretical model involving a local form of the Kirchhoff's law that introduces a spatial dependence of the photon chemical potential accounting for the pumping of each active layer. Numerical simulations show the occurrence of a plasmon mediated energy transfer over distances of several μm between spatially separated inorganic emitters' ensembles and organic emitters' ensembles. The excellent agreement between model and experiments, for any size of the CPA, shows that this comprehensive method enables the interpretation of systems in which thermalized materials with different chemical potential couple within complex structures. Our findings pave the way towards a thorough investigation of the interactions, mediated by the electromagnetic environment, between materials out of thermodynamic equilibrium. This will open new avenues for the design and fabrication of new materials bringing together the best of organic and inorganic worlds.

Methods

Sample preparation

The sample is fabricated as follows. First, a continuous 50 nm thick silver film is evaporated onto a glass coverslip. Then, a layer of J-aggregates is deposited by spin-coating a solution of 5,6-Dichloro-2-[[5,6-dichoro-1-ethyl-3-(4-sulfobutyl)-benzimi-dazol-2-ylidene]-propenyl]-1-

ethyl-3-(4-sulfobutyl)-benzimidazolium hydroxide, inner salt, sodium salt (TDBC) in distilled water with a concentration of 8.6 mM. At this stage, we performed the UV-lithography to obtain circularly photobleached areas. Finally, we deposited on top a layer containing CdSe core CdS/CdZnS/ZnS multishell QDs embedded in a transparent Poly(methyl methacrylate) (PMMA) matrix. For this layer, we prepare a solution of the QDs in toluene with a concentration of $\sim 1\,\mu$M in which transparent PMMA was added to the solution at a mass concentration of 0.5%. The solution was homogeneously deposited by spin coating and the QDs concentration was established so that the emitters are homogeneously dispersed in the layer. Note that the solvents are different for the J-aggregated TDBC and the QDs in order to avoid dissolving the first layer when the second layer is spin-coated. The thicknesses of the layers were determined by AFM topography measurements resulting in 17 nm for the TDBC J-aggregates and 15 nm for the QDs/PMMA layer.

Theoretical model and simulations

Brendel-Bormann model for refractive indexes of fluorophores

In order to describe the flurophores' layers and compute the absorbed power and thus the photoluminescent emission (1), it is necessary to have a permittivity model for each layer of emitters that accounts for the inhomogeneous broadening of the transitions for each layer of emitters (see a discussion in ref[24]). We use Brendel-Bormann models[25–27] for each layer and adjust the parameters of the models by using the same procedure as the one described in ref.[24] The Brendel-Bormann expression is reminded below:

$$\epsilon(\omega) = \epsilon_{\mathrm{bg}} + \sum_{k=1}^{m} X_{\mathrm{k}}(\omega), \tag{2}$$

where X_{k} is an infinite sum of Lorentz oscillators whose amplitudes are given by a Gaussian function:

$$X_{\mathrm{k}}(\omega) = \frac{1}{\sqrt{2\pi}\sigma_{\mathrm{k}}} \int_{-\infty}^{+\infty} dx \exp\left(-\frac{(x-\nu_{0\mathrm{k}})^2}{2\sigma_{\mathrm{k}}^2}\right) \frac{\nu_{\mathrm{pk}}^2}{x^2 - \omega^2 - i\nu_{\tau\mathrm{k}}\omega}. \tag{3}$$

To find the parameters of the J-aggregated TDBC model of permittivity, we use the photoluminescent map from the system made of the silver and molecules layers, before the bleaching and before the QDs' deposition. The experimental data as well as the parameters of the model are identical to the parameters used in ref.[24] The TDBC layer displays some anisotropy, so that we introduce the refractive index of the molecules in the perpendicular direction of the layer (denoted $n_\perp$) as an additional constant parameter of the cost function $f_{\text{cost}}(\epsilon)$ (see ref.[24]).

We model the CPA by a medium of homogeneous refractive index within the bleached region. The index model is chosen as dispersion free, and does not display any excitonic transition. The permittivity model of both CPA and QDs are determined at the same time by an optimization process based on the fit of the photoluminescent map given in Fig. 3f, where the QDs are deposited on an infinite layer of bleached J-aggregated TDBC.

Before performing the optimization procedure, we first filter some noise by convoluting by a rectangular window function in the (λ,θ) plane whose widths are 6.2 nm and 2°. The values of the parameters are gathered in table 2.

Table 2: Brendel-Bormann model parameter values

Parameters	J-aggregates			bleached J-aggregates	QDs	
	k=1	k=2	k=3	/	k=1	k=2
$\nu_{0\text{k}}$ (eV)	2.07	2.14	2.17	/	2.22	2.76
$\nu_{\tau\text{k}}$ (eV)	1.14e-09	1.46e-13	2.10e-06	/	3.83e-12	3.72e-11
ν_{pk} (eV)	0.10	1.44	0.25	/	0.013	0.83
σ_{k} (eV)	0.025	0.025	0.070	/	0.042	0.13
ϵ_{bg}		2.83		2.13	3.18	
$n_\perp$		2.82		/	/	

Approximations in the local Kirchhoff's law

Two approximations of Eq.1 have been made to compute the PL of Fig. 3 g-l. Firstly, $\mu(\mathbf{r}')$ was considered to be a non-zero constant in the volume of excited emitters and zero everywhere else, as can be shown in Fig. 2b, where the hatched areas correspond to the volumes

of excited emitters.

Let us first discuss the volume of emitting QDs. Experimentally, the excitation laser frequency was selected to pump preferentially the QDs. The volume of excited QDs is thus defined by the laser spot size, here a disk of diameter $\Phi_{\mathrm{QDs}} = 500\,\mathrm{nm}$. We verified that the quantum dots cannot be re-excited by the surface plasmon launched by the QDs at 570 nm (the QDs' emission wavelength). To do that, we consider the system described in Fig. 1a and 3f, when the TDBC layer is entirely bleached. We compare the intensity decay length of the plasmon (defined as $1/(2k'')$) with and without the QDs. If the decay length does not change significantly, most of the absorption is due to the metal so that multiple absorption-emission processes cannot take place. In other words, we compute the decay length of the surface plasmon when the QDs' layer is described by a BB refractive index described in Table 2. We obtain $\delta_1 = 2.21$ μm. We then discard the resonance of the QDs by replacing its refractive index by its background contribution only i.e. $n_{\mathrm{BQbg}} = 1.78$. The decay length slightly increases to $\delta_2 = 2.36$ μm without the absorption of the QDs. This tiny increase of the decay length points out that the absorption by the QDs is too low to display any absorption - reemission process. The QDs are thus only excited in the volume defined by the laser spot size.

Regarding the volume of excited J-aggregated TDBC molecules, it was defined following observations and interpretations from the experimental data from Fig 3b-f. In these cases, the molecules are photobleached over areas larger than Φ_{QDs} (except for Fig 3a and 3g), and can be excited directly neither by the QDs nor by the excitation laser. *However, it was necessary to include a nonzero chemical potential for the molecules to reproduce theoretically the experimental data of light emission in Fig. 3g-i. We interpret this observation by considering that the J-aggregated molecules are excited by the QDs through the surface plasmons.* In a rigorous manner, we should take into account all the J-aggregated molecules outside the bleached area. However, for numerical computation, we had to take into account a finite volume of diameter Φ_{Jagg} of excited molecules, where we consider that all the molecules are

excited inside and none outside ($\mu_{\text{Jagg}}(\rho) = 0$ for $\rho > \Phi_{\text{Jagg}}/2$, Fig. 2b). We identify 3 different cases :

1. The case where the QDs are deposited on top of an infinite layer of active J-aggregated molecules (Fig. 3a). In that case, $\Phi_{\text{Jagg}} = 2\delta_a$, where $\delta_a = 1.21$ μm is the intensity decay length of the upper polariton at 570 nm.

2. The case where the molecules are photobleached over areas larger than Φ_{QDs}, with $\Phi_{\text{CPA}} < 2\delta_1$ (Fig 3 b-c), with $\delta_1 = 2.21$ μm defined earlier as the decay length of the surface plasmon at 570 nm, launched by the QDs on top of a bleached area of molecules. In that case, $\Phi_{\text{Jagg}} = 2(R_{\text{CPA}} + \delta_a)$.

3. For configurations where the CPA is larger than $2\delta_1$ (Fig 3 d-f with $\Phi_{\text{CPA}} = 5$, 8 and 40 μm, respectively), we could recover the experimental data without including a contribution of the molecules so that $\Phi_{\text{Jagg}} = 0$.

This choice of effective volume with a constant value of μ_{Jagg} is equivalent to the computation of the absorption over the entire volume when assuming that the number of excited molecules decays exponentially as $\frac{1}{r}\exp(-r/\delta_a)$.
The values of the diameter Φ_{Jagg} of the volume of excited TDBC are presented in table 3.

Table 3: Values of the effective diameters Φ_{Jagg}

	unbleached	$\Phi_{\text{CPA}} = 1$ μm	$\Phi_{\text{CPA}} = 2$ μm	$\Phi_{\text{CPA}} \geq 5$ μm
Φ_{Jagg} (μm)	2.4	3.4	4.4	0

Finally, the Wien's approximation is valid at 300K and states that $\exp(\frac{\hbar\omega - \mu(\mathbf{r}')}{k_B T}) >> 1$ and the medium is considered homogeneous over the entire volumes of the different layers, and defined by its temperature T.

With these assumptions, Eq. (1) can be simplified and rearranged as the sum of the two contributions due to the QDs and the molecules. We remind that the molecules are placed

between the silver layer and the QDs layer. We obtain :

$$dP_{\mathrm{e}}^{(l)}(\mathbf{u},\lambda) = d\lambda d\Omega[dP_{\mathrm{abs}}^{\mathrm{Jagg}}(-\mathbf{u},\lambda)\mathrm{I}_{\mathrm{BB}}(\lambda)\mathrm{e}^{\frac{\mu_{\mathrm{Jagg}}}{k_B T}} + dP_{\mathrm{abs}}^{\mathrm{QDs}}(-\mathbf{u},\lambda)\mathrm{I}_{\mathrm{BB}}(\lambda)\mathrm{e}^{\frac{\mu_{\mathrm{QDs}}}{k_B T}}], \tag{4}$$

with

$$dP_{\mathrm{abs}}^{i}(-\mathbf{u},\lambda) = \varphi_{\mathrm{inc}} \int_{V_i} d^3\mathbf{r}' \alpha^{(l)}(-\mathbf{u},\mathbf{r}',\lambda), \tag{5}$$

and

$$\mathrm{I}_{\mathrm{BB}}(\lambda) = \frac{1}{\lambda^5} \frac{1}{\exp(\frac{hc}{\lambda k_B T})}. \tag{6}$$

After factorisation and normalization by the maximum emitted power at λ_0 and $\mathbf{u_0}$, Eq. 4 becomes:

$$\frac{dP_{\mathrm{e}}^{(l)}(\mathbf{u},\lambda)}{dP_{e}^{(l)}(\mathbf{u_0},\lambda_0)} = \frac{\mathrm{I}_{\mathrm{BB}}(\lambda)}{\mathrm{I}_{\mathrm{BB}}(\lambda_0)} \frac{dP_{\mathrm{abs}}^{\mathrm{Jagg}}(-\mathbf{u},\lambda) + dP_{\mathrm{abs}}^{\mathrm{QDs}}(-\mathbf{u},\lambda)\mathrm{e}^{\frac{\Delta\mu}{k_B T}}}{dP_{\mathrm{abs}}^{\mathrm{Jagg}}(-\mathbf{u_0},\lambda_0) + dP_{\mathrm{abs}}^{\mathrm{QDs}}(-\mathbf{u_0},\lambda_0)\mathrm{e}^{\frac{\Delta\mu}{k_B T}}}, \tag{7}$$

with $\Delta\mu = \mu_{\mathrm{QDs}} - \mu_{\mathrm{Jagg}}$. This factor $\Delta\mu$ is adjusted to fit the experimental emission. For $\Phi_{\mathrm{CPA}} > 2\delta_1$, $\Delta\mu = \mu_{\mathrm{QDs}}$ and $dP_{\mathrm{abs}}^{\mathrm{Jagg}}(-\mathbf{u},\lambda)$ is null. Only the QDs contribute to the photoluminescent emission in this latter case.

Thicknesses identification

Once refractive indexes for J-aggregated TDBC, bleached J-aggregated TDBC and QDs are extracted from the optimization procedure for each type of emitters separately, it is possible to compute the emission of the whole system composed of QDs on active and bleached J-aggregated TDBC, on top of the silver layer.

We used the system without bleached molecules (Fig. 3g) to adjust the thickness of the different layers to fit the experimental branches positions. We found $t_{\mathrm{Jagg}}^{th} = 11$ nm and $t_{\mathrm{QDs}}^{th} = 15$ nm, which is consistent with the experimental atomic force microscopy measurements ($t_{\mathrm{Jagg}} = 17$ nm and $t_{\mathrm{QD}} = 15$ nm). These values were kept the same for all CPA configurations

(Fig 3h-l, matching Fig 3b-f).

Acknowledgments

The authors would like to thank Thomas Pons and Sandrine Ithurria for the fabrication and supply of the quantum dots.

Funding Sources

French Agence Nationale pour la Recherche Grant No. ANR-18-CE30-0014 PlasHybrid and Grant No. ANR-17-CE24-0046.

European Union's Horizon 2020 research and innovation programme under the Marie Sklodowska-Curie grant agreement No. 754387.

LABEX WIFI (Laboratory of Excellence within the French Program "Investments for the Future") under references ANR-10-LABX-24 and ANR-10-IDEX-0001-02 PSL.

J.-J.G. acknowledges the support of Institut Universitaire de France.

References

(1) Gish, M. K.; Pace, N. A.; Rumbles, G.; Johnson, J. C. Emerging Design Principles for Enhanced Solar Energy Utilization with Singlet Fission. *The Journal of Physical Chemistry C* **2019**, *123*, 3923–3934.

(2) Harris, R. D.; Bettis Homan, S.; Kodaimati, M.; He, C.; Nepomnyashchii, A. B.; Swenson, N. K.; Lian, S.; Calzada, R.; Weiss, E. A. Electronic Processes within Quantum Dot-Molecule Complexes. *Chemical Reviews* **2016**, *116*, 12865–12919, PMID: 27499491.

(3) Huang, Z.; Tang, M. L. Designing Transmitter Ligands That Mediate Energy Transfer between Semiconductor Nanocrystals and Molecules. *Journal of the American Chemical Society* **2017**, *139*, 9412–9418, PMID: 28640637.

(4) Voznyy, O.; Sutherland, B. R.; Ip, A. H.; Zhitomirsky, D.; Sargent, E. H. Engineering charge transport by heterostructuring solution-processed semiconductors. *Nature Reviews Materials* **2017**, *2*, 17026.

(5) Agranovich, V. M.; Gartstein, Y. N.; Litinskaya, M. Hybrid Resonant Organic-Inorganic Nanostructures for Optoelectronic Applications. *Chemical Reviews* **2011**, *111*, 5179–5214.

(6) Steiner, A. M.; Lissel, F.; Fery, A.; Lauth, J.; Scheele, M. Prospects of Coupled Organic-Inorganic Nanostructures for Charge and Energy Transfer Applications. *Angewandte Chemie International Edition* **2021**, *60*, 1152–1175.

(7) Agranovich, V.; Benisty, H.; Weisbuch, C. Organic and inorganic quantum wells in a microcavity: Frenkel-Wannier-Mott excitons hybridization and energy transformation. *Solid State Communications* **1997**, *102*, 631–636.

(8) Dubovskiy, O.; Agranovich, V. To the theory of hybrid organics/semiconductor nanostructures in microcavity. *Solid State Communications* **2017**, *251*, 66–72.

(9) Paschos, G. G.; Somaschi, N.; Tsintzos, S. I.; Coles, D.; Bricks, J. L.; Hatzopoulos, Z.; Lidzey, D. G.; Lagoudakis, P. G.; Savvidis, P. G. Hybrid organic-inorganic polariton laser. *Scientific Reports* **2017**, *7*, 11377.

(10) Slootsky, M.; Liu, X.; Menon, V. M.; Forrest, S. R. Room Temperature Frenkel-Wannier-Mott Hybridization of Degenerate Excitons in a Strongly Coupled Microcavity. *Phys. Rev. Lett.* **2014**, *112*, 076401.

(11) Agrawal, A. K.; Sahu, P. K.; Seth, S.; Sarkar, M. Electrostatically Driven Förster Resonance Energy Transfer between a Fluorescent Metal Nanoparticle and J-Aggregate in an Inorganic-Organic Nanohybrid Material. *The Journal of Physical Chemistry C* **2019**, *123*, 3836–3847.

(12) Asgar, H.; Jacob, L.; Hoang, T. B. Fast spontaneous emission and high Förster resonance energy transfer rate in hybrid organic/inorganic plasmonic nanostructures. *Journal of Applied Physics* **2018**, *124*, 103105.

(13) Bouchet, D.; Cao, D.; Carminati, R.; De Wilde, Y.; Krachmalnicoff, V. Long-range plasmon-assisted energy transfer between fluorescent emitters. *Physical Review Letters* **2016**, *116*, 037401.

(14) Bouchet, D.; Lhuillier, E.; Ithurria, S.; Gulinatti, A.; Rech, I.; Carminati, R.; De Wilde, Y.; Krachmalnicoff, V. Correlated blinking of fluorescent emitters mediated by single plasmons. *Physical Review A* **2017**, *95*, 033828.

(15) Greffet, J.-J.; Bouchon, P.; Brucoli, G.; Marquier, F. Light emission by nonequilibrium bodies: local Kirchhoff law. *Physical Review X* **2018**, *8*, 021008.

(16) Guebrou, S. A.; Symonds, C.; Homeyer, E.; Plenet, J.; Gartstein, Y. N.; Agranovich, V. M.; Bellessa, J. Coherent emission from a disordered organic semiconductor induced by strong coupling with surface plasmons. *Physical Review Letters* **2012**, *108*, 066401.

(17) Chevrier, K.; Benoit, J.-M.; Symonds, C.; Saikin, S.; Yuen-Zhou, J.; Bellessa, J. Anisotropy and controllable band structure in suprawavelength polaritonic metasurfaces. *Physical Review Letters* **2019**, *122*, 173902.

(18) Bailly, E.; Hugonin, J.-P.; Vest, B.; Greffet, J.-J. Spatial coherence of light emitted by thermalized ensembles of emitters coupled to surface waves. *Physical Review Research* **2021**, *3*, L032040.

(19) Bellessa, J.; Bonnand, C.; Plenet, J.; Mugnier, J. Strong coupling between surface plasmons and excitons in an organic semiconductor. *Physical Review Letters* **2004**, *93*, 036404.

(20) Gassenq, A.; Chevrier, K.; Bard, A.; Benoit, J.-M.; Symonds, C.; Bellessa, J. Selective grating obtained by dye microstructuration based on local photobleaching using a laser writer. *Applied optics* **2020**, *59*, 5697–5701.

(21) Lidzey, D.; Bradley, D.; Virgili, T.; Armitage, A.; Skolnick, M.; Walker, S. Room temperature polariton emission from strongly coupled organic semiconductor microcavities. *Physical Review Letters* **1999**, *82*, 3316.

(22) Hopfield, J. J. Theory of the Contribution of Excitons to the Complex Dielectric Constant of Crystals. *Phys. Rev.* **1958**, *112*, 1555–1567.

(23) Wurfel, P. The chemical potential of radiation. *J. Phys. C: Solid State Phys.* **1982**, *15*, 3967–3985.

(24) Bailly, E.; Chevrier, K.; de la Vega, C. P.; Hugonin, J.-P.; Wilde, Y. D.; Krachmalnicoff, V.; Vest, B.; Greffet, J.-J. Method to measure the refractive index for photoluminescence modelling. *Opt. Mater. Express* **2022**, *12*, 2772–2781.

(25) Brendel, R.; Bormann, D. An infrared dielectric function model for amorphous solids. *Journal of Applied Physics* **1992**, *71*, 1–6.

(26) Rakic, A. D.; AB, D.; JM, E.; ML, M. Optical properties of metallic films for vertical-cavity optoelectronic devices. *Applied optics* **1998**, *37*, 5271–83.

(27) Djorović, A.; Meyer, M.; Darby, B. L.; Le Ru, E. C. Accurate Modeling of the Polarizability of Dyes for Electromagnetic Calculations. *ACS Omega* **2017**, *2*, 1804–1811, PMID: 31457544.

TOC Graphic

For Table of Contents Use Only
Title: "Plasmon mediated energy transfer between two systems out of equilibrium"
Authors: Camilo R. Pérez de la Vega, Elise Bailly, Kévin Chevrier, Benjamin Vest, Jean-Paul Hugonin, Antoine Bard, Alban Gassenq, Clémentine Symonds, Jean-Michel Benoit, Joel Bellessa, Jean-Jacques Greffet, Yannick De Wilde, Valentina Krachmalnicoff.

Synopsis: This graphic depicts a multi-layered sample composed of a glass substrate with a silver film, a layer of J-aggregates, and a layer of quantum dots deposited on it. When a blue laser is directed through the substrate towards a region of the sample where the J-aggregates have undergone photobleaching, the quantum dots layer is excited. Energy transfer between quantum dots and J-aggregates mediated by surface plasmon polaritons can be studied by taking advantage of the microstructuration of the multilayered sample.